

## Giant impacts, core stratification, and failure of the Martian dynamo

Jafar Arkani-Hamed<sup>1,2</sup> and Peter Olson<sup>3</sup>

Received 26 January 2010; accepted 24 March 2010; published 30 July 2010.

[1] The close timing of the giant impacts and the cessation of the core dynamo of Mars at around 4 Ga suggest a possible causal relationship between these two events. We study the shock heating of the Martian interior caused by the impact that created Utopia basin, the largest of the 20 giant impact basins formed on Mars around 4 Ga. Using empirical scaling laws connecting the diameters of the basin and the projectile, we calculate the shock pressure distribution in Mars on the basis of Pierazzo et al.'s (1997) formula, which is then used to estimate the impact-induced temperature increase in the Martian mantle and core, adopting the “ordinary” and “foundering” shock heating mechanisms proposed by Watters et al. (2009) and impact velocities of 10 and 15 km/s. It is shown that the reduction of the heat flux out of the core due to impact heating of the overlying mantle is on the order of 0.03%–0.3% of the preimpact heat flux of the core (15 mW/m<sup>2</sup>), indicating that the impact heating of the mantle has insignificant effect on the thermal convection of the core. However, the shock waves that penetrate into the core directly and differentially heat the core in only a few minutes, which causes stable thermal stratification of the core within about a few years and diminishes the core convection and the thermally driven core dynamo within a few thousand years. Exhaustion of the impact heat and removal of the stratification is necessary to reestablish a superadiabatic temperature gradient and reactivate convection in the core. As the impact heat becomes concentrated in the upper parts of the core, the stratified part of the core first cools by conduction to the mantle and then later with a contribution from penetrative convection below the core–mantle boundary and by conduction into the deeper parts of the core. Depending on the impact velocity and the shock heating mechanisms, tens of millions of years may be needed to fully exhaust the core heat to the mantle, during which time global core convection is suppressed and a thermally driven core dynamo is problematic.

**Citation:** Arkani-Hamed, J., and P. Olson (2010), Giant impacts, core stratification, and failure of the Martian dynamo, *J. Geophys. Res.*, 115, E07012, doi:10.1029/2010JE003579.

### 1. Introduction

[2] The lack of a global scale magnetic field of Mars at present and the strong magnetic anomalies of Martian crust detected by Mars Global Surveyor (MGS) [Acuña et al., 1999] point to a now-extinct dynamo in Mars in the distant past. Estimates of the paleointensity of the Martian magnetic field based on the oldest Martian meteorite ALH84001 [e.g., Weiss et al., 2008] indicate a core field intensity comparable to that in the present-day Earth, consistent with dynamo field intensity predictions based on a magnetostrophic force balance in its liquid core [Arkani-Hamed, 2005a]. Rock

magnetic analyses indicate that ALH84001 acquired its magnetization on Mars prior to 4 Ga [e.g., Weiss et al., 2002; Antretter et al., 2003].

[3] The absence of strong magnetic anomalies associated with the giant impact basins Utopia, Hellas, Isidis, and Argyre and with the Tharsis bulge and Elysium Rise or with the Valles Marineris Canyon and Arsia, Ascraeus, Olympus, and Pavonis mountains suggests that the source field and, by implication, the dynamo of Mars either waned or failed around 4 Ga [e.g., Arkani-Hamed, 2004; Johnson and Phillips, 2005]. The observations that many giant impact basins that formed at around 4.2–4.1 Ga such as Acidalia, Chryse, and Daedalia have appreciable magnetic anomalies, while those formed at later times about 4.1–3.9 Ga such as Utopia, Hellas, Isidis, and Argyre have weak anomalies or none at all, suggest the core dynamo waned during this time [Lillis et al., 2008]. The causes of dynamo failure are poorly understood and constitute outstanding problem for the early evolution of Mars.

[4] The assumption that terrestrial planet dynamos are driven by convection in their iron-rich liquid cores [e.g.,

<sup>1</sup>Department of Physics, University of Toronto, Toronto, Ontario, Canada.

<sup>2</sup>Earth and Planetary Sciences, McGill University, Montreal, Quebec, Canada.

<sup>3</sup>Earth and Planetary Sciences, Johns Hopkins University, Baltimore, Maryland, USA.

[Gubbins *et al.*, 1979] is so widespread that dynamo action in Mars is commonly equated with thermal convection in its core, even though other, nonconvective dynamo mechanisms are possible [Arkani-Hamed *et al.*, 2008; Arkani-Hamed, 2009] and the existence of core convection early in Mars history is far from assured. For example, many thermal evolution models of Mars [e.g., Stevenson *et al.*, 1983] are equivocal about core convection, partly because of the lack of pertinent information about the physical properties of Martian interior but partly because reasonable physical parameter choices allow for both convective and nonconvective states.

[5] In spite of this fundamental uncertainty, most models for the origin and demise of the Martian dynamo assume a convective state sometime in its early history. Nimmo and Stevenson [2000] propose a transient episode of plate tectonics strongly cooled the core and allowed a thermal convection dynamo for a time. Following this episode of plate tectonics, assumed to have lasted about 500 Myr, Mars became a one-plate planet with sluggish mantle convection and reduced heat loss from the core, and its dynamo failed. However, there is little evidence for such a plate tectonics episode on Mars [e.g., Pruis and Tanaka, 1995; Zuber, 2001]. Specifically, the proximity of the crater density of the lowland was formed in the later stages of the planetary accretion or shortly after [e.g., Frey *et al.*, 2002] and no plate tectonics have occurred since then. In addition, Breuer and Spohn [2003] showed that early plate tectonics on Mars is incompatible with its thick crust and the inferred monotonic decrease in crust production rate [see Hauck and Phillips, 2002] and therefore concluded that Mars has always been a one-plate planet.

[6] Even short-lived convective dynamo action in a one-plate planet the size of Mars is problematic, however, without the assistance of an inner core. Thermal evolution models of Mars with a permanent stagnant lid and no core superheat show that radioactive heat production in the mantle raises the mantle temperature and inhibits core cooling for the first 500 Myr [Breuer and Spohn, 2003; Williams and Nimmo, 2004; Arkani-Hamed, 2005b]. A possible remedy to this problem is to invoke core superheat. In order to maintain a thermal convective dynamo with a stagnant lid mantle, a core super heat of 150–250 K would be needed [Breuer and Spohn, 2003; Williams and Nimmo, 2004].

[7] Progressive solidification of Mars core has also been proposed to explain the dynamo origin [Young and Schubert, 1974; Schubert *et al.*, 2000]. Once again, however, there is no evidence of core solidification in the first 500 Myr of Mars history [e.g., Breuer and Spohn, 2003; Williams and Nimmo, 2004]. Furthermore, the time required for the core to solidify is expected to be far longer than 500 Myr [e.g., Schubert *et al.*, 1992; Williams and Nimmo, 2004].

[8] Other models explain the failure of the Martian dynamo in terms of its response to perturbations, including impact heat deposited in the mantle and later conducted into the core [Roberts *et al.*, 2009], direct heating of the core by impacts [Arkani-Hamed and Olson, 2010], and satellite infall [Arkani-Hamed *et al.*, 2008]. It is important to note that these perturbations can have lasting effects on the dynamo, even if they are relatively small. Kuang *et al.* [2008] showed that if Martian dynamo happened to be in a subcritical convective state (that is, convecting with a subcritical thermal gradient

because of the destabilizing effect of its magnetic field), then a very small perturbation, equivalent to a reduction of the heat flux at the core-mantle boundary by only 1%, could terminate the dynamo.

[9] Roberts *et al.* [2009] investigated the heating of Martian mantle by the impacts that created the 20 giant impact basins on Mars between 4.2 and 3.9 Ga, as reported by Frey [2008]. Roberts *et al.* [2009] showed that mantle heating by each of the impacts that created Arisia, Acidalia, Daedalia and Utopia basins was capable of reducing the heat flux at the core-mantle boundary enough to terminate a subcritical convective dynamo. They also speculated that a succession of impacts might be strong enough to terminate a supercritical dynamo by this mechanism.

[10] More recently, Arkani-Hamed and Olson [2010] showed that the direct heating of the core by the shock wave pressure of a giant impact produces lateral temperature variations of order of 100 K, far larger than the lateral temperature variations associated with core convection. They showed how such large temperature variations catastrophically overturn and stratify the core, suppressing convection and extinguishing a preexisting dynamo within a few tens of kiloyears.

[11] In this paper, we examine the shock heating of the Martian mantle and core by a giant impact. We consider an impact large enough to form the 3380 km diameter Utopia basin, the largest among the 20 giant impact basins formed at around 4 Ga, which provides upper limits on the impact heating of the mantle, its effect on the heat flux at the core-mantle boundary, and the impact heating of the core itself.

[12] Section 2 compares different models for the impact-induced temperature increase in the mantle. Section 3 addresses the direct heating of the core by the shock wave. Section 4 analyzes the thermal stratification of the core and the possibility of the cessation of a preexisting thermally driven core dynamo. Section 5 shows how a stratified core cools and how long it takes for a global convection to be reestablished and a strong core dynamo possibly be regenerated. Section 6 discusses the effects of certain assumptions made in this study.

## 2. Impact Heating of the Mantle

[13] Giant impacts on terrestrial planets not only excavate large portions of crust and mantle creating giant impact basins, they also produce shock waves that heat the mantle and core. In this and subsequent sections, we name the impacting body after the basin it created. Our focus here is on the Martian Utopia impact, although the theory is generally applicable to any terrestrial type giant impact.

[14] We first estimate the impact-induced shock wave pressure distribution in Mars due to a giant impact, parameterized in terms of its final basin size. We assume that the final basin diameter  $D_b$  is related to its transient (initial) diameter  $D_{tr}$  according to

$$D_b = 1.02 D_*^{-0.086} D_{tr}^{1.086} \quad (1)$$

[Holsapple, 1993] and that the transient diameter is related to the diameter of the impacting body  $D_{imp}$  according to

$$D_{imp} = 0.69 D_{tr}^{1.28} U^{-0.56} g_s^{0.28} \quad (2)$$

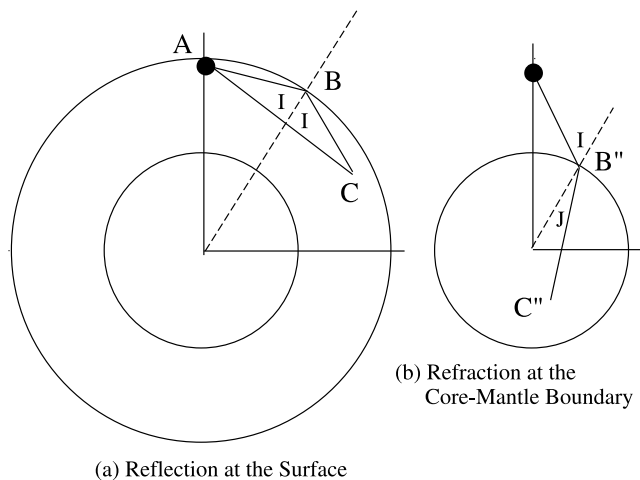


**Figure 1.** Schematic diagrams showing the direct and reflected rays of the shock wave. (a) Direct wave in the mantle travels along AC, the reflected wave travels from A, the center of the isobaric sphere, to B at the surface and then reflects and travels from B to C. The large black dot shows the isobaric sphere, and the dashed circle is the core-mantle boundary. (b) The shock wave propagates as a spherical wave and enters the core as it impinges the core-mantle boundary. I is the incident angle, and J is the refraction angle. The shock wave travels from A to B'' in the mantle and then from B'' to C'' in the core.

[Melosh, 1989].  $D_*$  is the transition diameter from simple to complex crater structures (approximately 7000 m for Mars),  $U$  is the impact velocity (in m/s), and  $g_s$  is the gravitational acceleration at the surface. The geometry of the impact is shown in Figure 1 and Table 1 gives values for the physical parameters used in this study.

[15] Following impact, a nearly uniform shock pressure  $P_s$  is generated inside the so-called isobaric sphere of radius  $r_c$ . According to Melosh [1989], this shock pressure is given by

$$P_s = \rho_m(C_m + S_m u_0)u_0, \quad r < r_c \quad (3a)$$

where  $\rho_m$  and  $C_m$  are the preshocked density and acoustic velocity of the mantle,  $u_0$  is the particle velocity in the isobaric sphere ( $u_0 = U/2$ , assuming similar target and impacting materials),  $S_m$  is a constant,  $r$  is the distance from the center of the isobaric region, and  $r_c = 0.0525D_{\text{imp}}U^{0.211}$  is the spherical radius of the isobaric region, which is approximately equal to the depth of penetration of the impacting body.

[16] Several different models have been advanced for the shock pressure distribution outside the isobaric region. In this study, we adopt the average model of Pierazzo *et al.* [1997]. The impact pressure is expressed as

$$P_s(r) = P_s(r_c) \cdot (r_c/r)^n, \quad r > r_c; n = -9.67 + 2.61 \log U. \quad (3b)$$

Note that the exponent  $n$  defined in (3b) is the same as that of Pierazzo *et al.* [1997], except that we use m/s for the impact velocity  $U$ , to be consistent with the SI units used in this paper. We emphasize that the decay of shock pressure with radius in this model is slower than those of most other models,

and the far-field shock heating is correspondingly higher than most other models (see section 6).

[17] The axisymmetric shock pressure in the planet interior is calculated using (3a) and (3b) at  $1 \times 1$  km grid intervals in a spherical coordinate system with the symmetry axis defined by the impact site and planet center (Figure 1). The pressure reduction near the surface due to interference of the direct and reflected waves is taken into consideration after modifying Melosh's [1989] rectangular coordinate algorithm to a spherical coordinate algorithm. This modification has appreciable effects on the location of the interference zone, where the direct and reflected waves interfere to reduce the effective shock pressure [Louzada and Stewart, 2009]. At the surface, the entire incident pressure wave reflects with a  $180^\circ$  phase shift. At the core-mantle boundary, the incident pressure wave is partly reflected to the mantle and partly transmitted to the core according to Snell's law. The interference of the direct and reflected waves in the mantle near the core-mantle boundary has only minor effects on the shock pressure and is neglected. We describe the core heating by the transmitted shock wave in section 3.

[18] As shock wave propagates, the material is first compressed then decompressed adiabatically; during decompression, a large fraction of the energy of compression is converted into kinetic energy, which results in the excavation of the impact basin. Much of the remaining energy of compression is converted into heat [Bjorkman and Holsapple, 1987]. Watters *et al.* [2009] have recently proposed three models for the irreversible temperature increase  $\Delta T$  due to the shock heating, which they term "ordinary," "climbing," and "foundering." The "ordinary" model adopts a uniform density mantle ( $\rho_0$ ) and assumes that the preshocked material is at zero pressure in the Hugoniot equations, whereas the "foundering" model includes the lithostatic pressure in the equations. The "climbing" model accounts for the changes in the Hugoniot equations due to lithostatic pressure and depth-dependent density in the mantle. The "ordinary" model yields the largest temperature increase, whereas the "foundering"

**Table 1.** Physical Parameters Common Among the Models

$R$ = Mars radius	3390 (km)
$R_c$ = Core radius	1700 (km)
$D_b$ = Basin diameter	3380 (km)
$G$ = Gravity at the surface	3.72 ( $\text{m/s}^2$ )
$\rho_i$ = Impactor density	3000 ( $\text{kg/m}^3$ )
$\rho_0$ = Mantle density	3500 ( $\text{kg/m}^3$ )
$\rho_c$ = Core density	7500 ( $\text{kg/m}^3$ )
$C_m$ = $P$ wave velocity in the mantle	7.24 (km/s)
$C_c$ = $P$ wave velocity in the core	4 (km/s)
$V_{sm}$ = $S$ wave velocity in the mantle	4 (km/s)
$S_m$ = The constant in equation (3a) for the mantle	1.25
$S_c$ = The constant in equation (3a) for the core	1.6
$C_{pm}$ = Specific heat of the mantle	1200 (J/kg/K)
$C_{pc}$ = Specific heat of the core	600 (J/kg/K)
$\alpha$ = Thermal expansion coefficient of the core	$10^{-5}$ (1/K)
$K_m$ = Thermal conductivity of the mantle	4 (W/m/K)
$K_c$ = Thermal conductivity of the core	40 (W/m/K)
$q_c$ = Mean heat flux at the core-mantle boundary	15 ( $\text{mW/m}^2$ )
$\nu$ = Kinematic viscosity of the core	from $10^{-4}$ to $10^4$ ( $\text{m}^2/\text{s}$ )

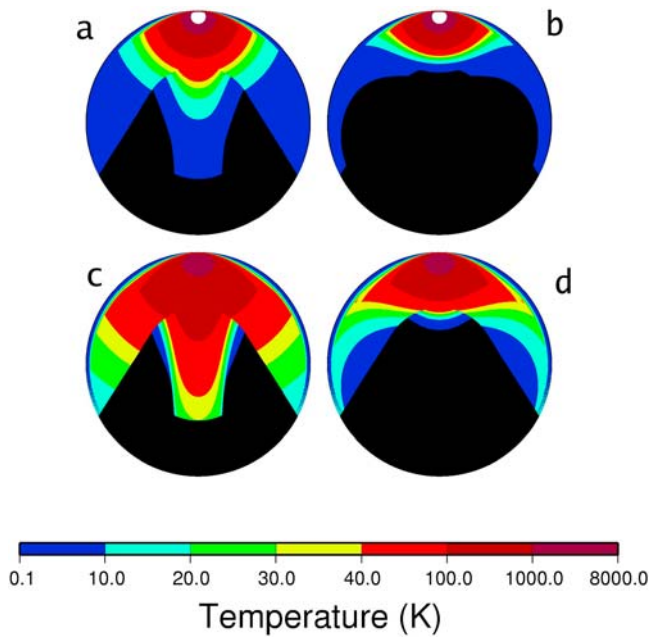


**Figure 2.** Calculated temperature increase produced in the mantle and the core of Mars by the shock wave heating following the Utopia impact. First row is for an impact velocity of 15 km/s, and the second row is for an impact velocity of 10 km/s. First column is for the “ordinary” shock heating model, and the second column is for the “foundering” shock heating model. The small white circles in the first row are slightly higher temperatures than the saturation temperature of 8000 K. No attempt is made to incorporate the latent heat of melting and evaporation near the impact site. The black areas in the first column do not receive any shock wave. The temperature increase is below 1 K in the additional black areas in the second column. This additional area arises because the lithostatic pressure reduces the effective shock pressure. The heating of the mantle by the shock wave emerging out of the core in the antipodal regions is insignificant and ignored here.

model yields the least temperature increase. The temperature increase by the “climbing” model is within the two others but closer to that of the “foundering” model [see *Watters et al.*, 2009, Figure 2]. In this study, we use both “ordinary” and “foundering” models as representative of the two extremes of the shock heating.

[19] For both models,  $\Delta T$  can be expressed in terms of the shock pressure and the lithostatic (hydrostatic) pressure  $P_o$  as [*Watters et al.*, 2009]

$$\Delta T = P_\delta(1 - 1/f)/(2\rho_o S) - (C/S)^2(f - \ln f - 1), \quad (4)$$

where

$$f = -P_\delta/\left(\beta\left\{1 - [(2P_\delta/\beta) + 1]^{1/2}\right\}\right), \quad (5)$$

$$P_\delta = P_s - P_o, \quad (6)$$

$$\beta = (C^2\rho_o)/(2S), \quad (7)$$

and the other symbols have their previous meanings. Equation (6) is for the “foundering” model. Setting the lithostatic pressure to zero in this equation yields the “ordinary” model. We calculate the lithostatic pressure distribution  $P_o$  using a simplified Mars model consisting of a uniform liquid core of radius 1700 km and density 7500 kg/m<sup>3</sup> and an overlying uniform mantle of radius 3390 km and density 3500 kg/m<sup>3</sup>. Our core radius is within the range of recent estimates, 1520–1840 km [*Yoder et al.*, 2003].

[20] Figure 2 shows the axisymmetric temperature increase in the mantle and core produced by the Utopia impact for the “ordinary” and “foundering” models, using equations (1)–(7) with the parameter values in Table 1. For comparative purposes, we consider two impact velocities:  $U = 10$  km/s, which is the average of the impact velocities of Mars proposed by *Neukum and Wise* [1976], and  $U = 15$  km/s, which is the velocity adopted by *Watters et al.* [2009] and *Roberts et al.* [2009]. Figure 2 shows the results for both models. Note that the temperatures calculated for the isobaric regions and their immediate surroundings are well above silicate melting temperatures and are therefore overestimates of the actual temperatures there, because the latent heats of melting and evaporation are not taken in to consideration.

[21] In this study, we are mainly interested in the impact-induced temperature increase near the core, where no shock melting occurs. Because the shock wave velocity in the liquid core is less than that in the solid mantle, part of the core (the shadow zone) receives no shock wave heating in either model. In addition, the impact heating of the mantle in the antipode side is not included in Figure 2, because by the time the shock wave propagating in the core reaches the core-mantle boundary in the antipode region, the shock pressure reduces substantially and heating of the mantle by the shock wave emerging out of the core is negligible. More importantly, Figure 2 demonstrates that the “ordinary” model results in appreciable temperature increase in the mantle close to the core-mantle boundary, whereas the temperature increase in the “foundering” model is much smaller there.

[22] Figure 3 shows the reduction of the heat flux at the core-mantle boundary because of impact heating of the mantle as a function of the colatitude measured from the subimpact point on the boundary. At a colatitude of  $\sim 54^\circ$ , the shock raypath is tangent to the core, and for larger colatitudes, the mantle immediately above the core receives no shock wave, except for the antipode region as mentioned above. The heat flux reduction in Figure 3 is calculated from Figure 2 using temperature differences at 5 and 10 km above the core-mantle boundary, respectively, to suppress adverse effects of small local fluctuations of temperature near the core-mantle boundary. This procedure yields smooth heat flow variations but slightly overestimates the impact-induced heat flux reduction at the core-mantle boundary because of the exponential decay of shock-induced temperature with depth. The numbers in the parentheses in Figure 3 are the mean (average) heat flux reduction for the entire surface of the core.

[23] For the case of a mean heat flux of  $\sim 15$  mW/m<sup>2</sup> at the core-mantle boundary immediately before the impact [*Roberts et al.*, 2009], the average reduction of heat flux is about 0.27% for the models with the “ordinary” shock heating and between 0.01% and 0.03% for the models with the “foundering” heating. These reductions are far below the

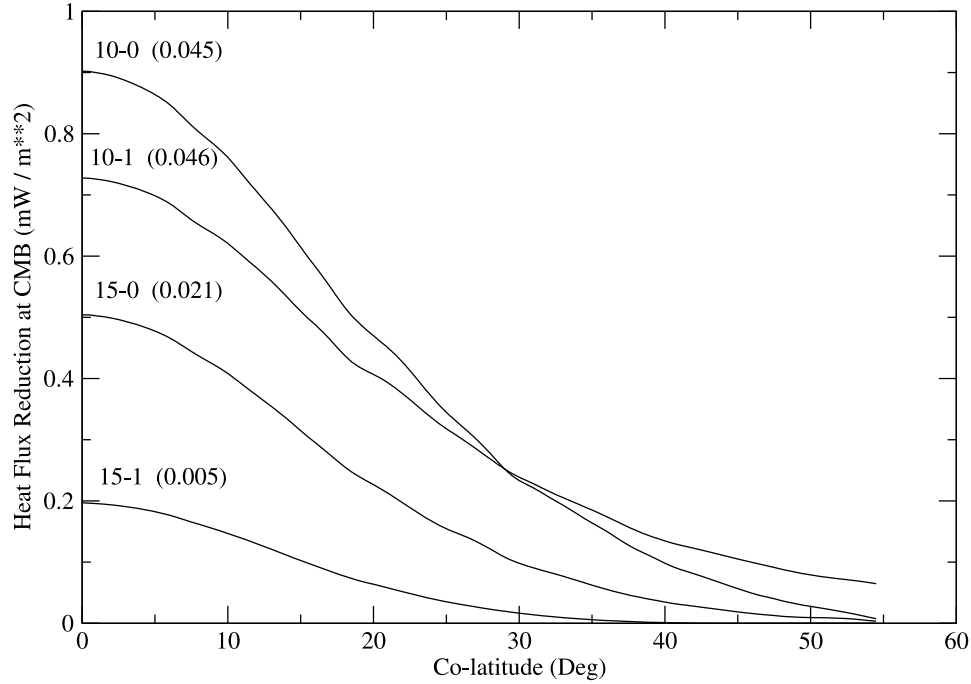


**Figure 3.** The heat flux reduction at the core-mantle boundary versus the colatitude relative to the sub-impact point. The first number on a curve is the impact velocity in km/s, and the second number denotes the shock heating model, 0 = “ordinary” and 1 = “foundering.” The numbers in the parentheses are the heat flux reduction in  $\text{mW}/\text{m}^2$  averaged over the entire area of the core-mantle boundary.

~1% heat flux reduction that *Kuang et al.* [2008] estimated for terminating a convective dynamo if it were in a subcritical state. The discrepancy is particularly evident for the “foundering” models, where the reduction in the heat flux at the core-mantle boundary is 30–100 times smaller than the 1% threshold. The same basic conclusion applies if the dynamo was in a supercritical convective state: the heat flux reduction of a fraction of a percentage would have negligible effects on the core dynamo. We note that the other giant basins created on Mars during this time are smaller than Utopia and are therefore expected to have less effect on the heat flux at the core-mantle boundary than what is shown in Figure 3. Accordingly, the heat flux reduction following shock heating of the mantle by a single giant impact seems incapable of terminating the core dynamo, although the effect of a sequence of impacts might be greater if impacts occurred at short time intervals.

### 3. Impact Heating of the Core

[24] The shock wave heating of the core is calculated with the same model as used in section 2 for the mantle. In the mantle, the shock propagates as a spherical wave from a focus at the center of the isobaric region. At the core-mantle boundary, part of the shock wave is transmitted to the core and the rest is reflected back into the mantle. We assume Snell’s law raypaths for the core-transmitted shock waves and calculate the refraction angle  $J$  of the transmitted ray according to

$$\sin(J) = \sin(I)V_c/V_m, \quad (8)$$

where  $I$  is the ray incident angle (see Figure 1b),  $V_c$  is the shock wave velocity in the core immediately below the core-mantle boundary, and  $V_m$  is the shock wave velocity in the mantle immediately above the core-mantle boundary. We use three different methods to calculate the shock wave velocity ratio  $\zeta (= V_c/V_m)$ : the impedance match method [*Watters et al.*, 2009], the shock dynamic equation applied across the core-mantle boundary [see *Han and Yin*, 1993, section 10.4], and seismic ray theory [see *Aki and Richards*, 2002, section 5.2].

[25] The impedance match method assumes that the shock pressure and particle velocity are continuous across the core-mantle boundary. Accordingly,  $V_m$  and  $V_c$  are determined by

$$V_m = C_m + S_m u_m, \quad (9)$$

$$V_c = C_c + S_c u_m, \quad (10)$$

where  $C_m$  and  $C_c$  are the bulk sound wave velocities of the mantle and core, assumed constant,  $S_m$  and  $S_c$  are constants, and  $u_m$  is the particle velocity immediately above the core-mantle boundary, which, according to this method, is equal to the particle velocity immediately below the boundary. Figure 4 shows the distribution of the particle velocity in the mantle, calculated using the power law decay model of *Peirazzo et al.* [1997], for which

$$u_m(r) = u_o(r_c/r)^{n'}, r > r_c; n' = -3.76 + 1.15 \log(U) \quad (11)$$

and that of the shock wave velocity  $V_m$ . The shock wave velocity ratio  $\zeta$  is found to be 0.66 and 0.65 for the impact velocities of  $U = 10$  and 15 km/s, respectively.

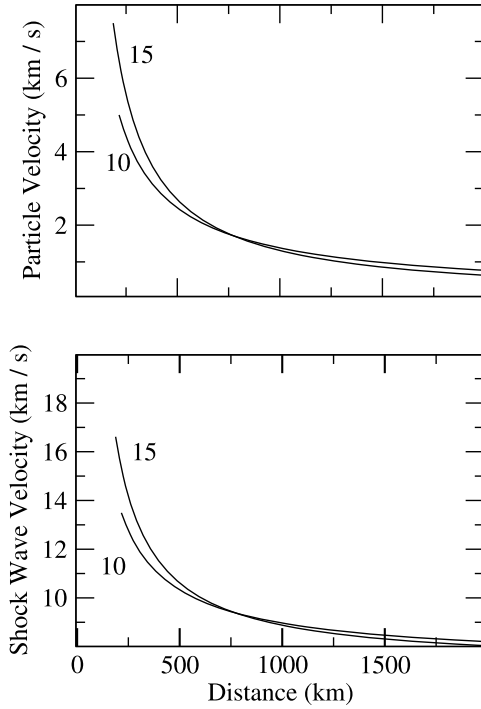


**Figure 4.** Particle velocity and shock wave velocity in the mantle as functions of the distance from the center of the isobaric sphere. The numbers on the curves denote the impact velocities in km/s.

[26] To apply the shock dynamic equation, we note that the lithostatic pressure is continuous at the core-mantle boundary and the specific heat ratio  $\gamma$  ( $= C_p/C_v$ ) is on the order of 1 ( $C_p$  and  $C_v$  are the specific heats at constant pressure and constant volume, respectively). Therefore, the shock dynamic equation simplifies to [Han and Yin, 1993, equation 10.7]

$$dM/M = \nu^2(1 - \eta \cot^2(I)) / [\cot^2(I) - \nu^2] dC/C, \quad (12)$$

where the Mach number  $M = V/C$  denotes the ratio of the shock wave velocity  $V$  to bulk sound velocity  $C$ ,

$$\begin{aligned} \nu^2 &= (M^2 - 1)K / (2M^2), \\ K &= 2\{1 + 2(1 - \mu^2) / [\mu(\gamma + 1)]\}^{-1} \{1 + 2\mu + 1/M^2\}^{-1}, \\ \mu &= \{[2 + M^2(\gamma - 1)] / [2M^2\gamma - (\gamma - 1)]\}^{1/2}, \\ \eta &= 1 + 2\mu(M^2 - 1) / [2 + M^2(\gamma - 1)], \end{aligned}$$

and  $dM$  and  $dC$  in (12) denote jumps in the Mach number and bulk sound velocities across the core-mantle boundary, respectively. Equation (12) is integrated across the core-mantle boundary from the incident angle  $I = 0-65^\circ$  at  $1^\circ$  intervals to obtain the shock wave velocity immediately below the boundary as a function of the colatitude relative to the subimpact point. The resulting shock wave velocity ratio  $\zeta$  varies from 0.58 at  $I = 0$  to 0.47 at  $I = 65^\circ$  for the impact velocity of 10 km/s and from 0.57 to 0.48 for the impact velocity of 15 km/s.

[27] We note that the magnitude of the particle velocity term in the right-hand side of (9) diminishes rapidly with distance from the isobaric focus and the shock wave velocity approaches the bulk sound velocity near the core-mantle

boundary (see Figure 4), resulting in the shock wave velocity ratio  $\zeta$  comparable to that of the acoustic velocity ratio  $C_m/C_c = 0.55$ . We also note that the impedance match and shock dynamic methods assumes the continuity of shock pressure across the boundary, whereas the seismic ray theory, while providing a good estimate for the shock wave velocity ratio  $\zeta$  (i.e., for the refraction angle), allows some part of the incident pressure wave to be transferred to reflected waves, yielding a smaller shock pressure amplitude immediately below the core-mantle boundary. Therefore, we adopt the ray theory to obtain a lower estimate for the shock heating in the core and calculate the refraction angle and the shock pressure immediately beneath the core-mantle boundary using equations 5.39 and 5.40 from Aki and Richards [2002]. Figure 5 shows the transmission coefficient of the shock pressure, the ratio of the transmitted pressure to the incident pressure, as a function of the incident angle  $I$ , indicating appreciable decrease of the shock pressure upon entering the core as the incident angle increases.

[28] The shock pressure  $P_{C''}$  at point  $C''$  in the core is given by (see Figure 1b)

$$P_{C''} = P_{B''} [AB'' / (AB'' + B''C'')]^n, \quad (13)$$

where  $P_{B''}$  is the shock pressure in the core immediately below the core-mantle boundary, and the impact heating is then calculated using (4). Because shock heating effects are only weakly dependent on the composition (silicate versus iron) and weakly dependent on the preshocked state of medium (solid versus liquid), we assume that (4) provides an adequate estimate of the shock heating in the core. Figure 6 shows the resulting temperature increase in the core for impact velocities of  $U = 10$  and 15 km/s and for the “ordinary” and “foundering” models, extracted from Figure 2 for better illustration. Figure 6 shows that, counterintuitively, the higher velocity impact heats the core less than the lower velocity impact, because the pressure in the shock wave produced by the higher velocity impact decays faster than that produced by the lower velocity impact, according to Pierazzo *et al.* [1997] model adopted in this study. Figure 6 also shows that the “foundering” model heats only a very limited region of the upper part of the core directly beneath the impact site, whereas the “ordinary” model heats the entire core, except the shadow regions where the shock wave cannot penetrate according to Snell’s law. In what follows, we use the “ordinary” model heating results for illustration purposes.

#### 4. Stratification of the Core and Failure of the Dynamo

[29] The shock-induced temperature perturbations shown in Figure 6 are far larger than the dynamical temperature perturbations associated with convection in iron-rich planetary cores, which are estimated to be much less than 1 K [e.g., Stevenson, 1987; Christensen and Wicht, 2007]. The short-term dynamical response of the liquid core to the thermal perturbations shown in Figure 6 consists of an energetic thermal wave adjustment that redistributes the shock-heated fluid onto spherically symmetric isothermal surfaces with increasing temperature as a function of distance from the center and results in a stable thermal stratification [Arkani-Hamed and Olson, 2010]. The resulting stratification is

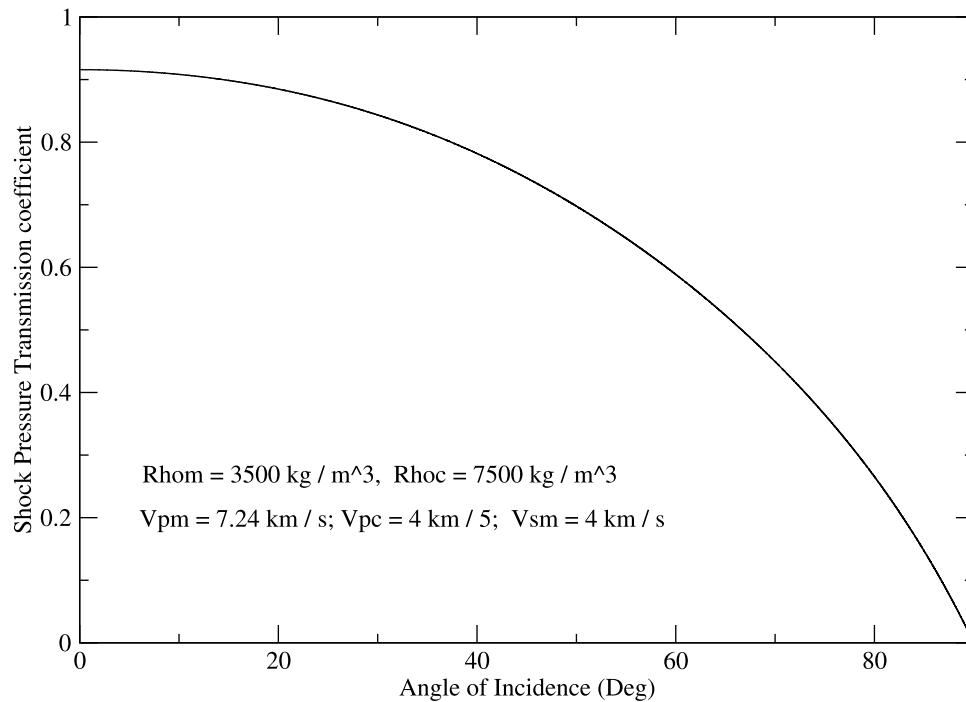


**Figure 5.** Pressure wave transmission coefficient (pressure of the refracted wave divided by the pressure of the incident wave) as a function of the incident angle  $I$  (Figure 1b) calculated using *Aki and Richards* [2002], equations (5.39) and (5.40).  $\rho_{\text{m}}$  and  $\rho_{\text{c}}$  are densities of the mantle and the core,  $V_{\text{pm}}$  and  $V_{\text{sm}}$  are the  $P$  and  $S$  wave velocities in the mantle, and  $V_{\text{pc}}$  is the  $P$  wave velocity in the core.

calculated assuming the redistribution process is adiabatic, which is likely to be a good approximation since the thermal wave velocities are very large and the adjustment time scale is very short. Figure 7 shows the spherically symmetric temperature distribution in the core after the stratification, where the impact temperature increase has been added to a preimpact adiabatic temperature profile with a reference value of 2000 K at the core-mantle boundary.

[30] If thermal convection was present in the core prior to the impact, the induced thermal stratification shown in Figure 7 would be sufficient to extinguish convection, particularly if the convection was driven by heat flux at the core-mantle boundary. Dynamo calculations show that a preexisting magnetic field in Mars core decays on a  $\sim 15$  kyr time scale under these conditions [*Arkani-Hamed and Olson, 2010*]. More generally though, the induced stratification works against dynamo action of any kind by inhibiting radial fluid motion, especially in the region below the core-mantle boundary where the stratification is initially strongest.

## 5. Resumption of the Core Convection

[31] The duration of the shock-induced thermal stratification event is an important issue. The core must exhaust the extra impact heat to the mantle before core convection can resume. We can estimate its duration and the time required to reestablish convection by considering the following thermal evolution of Mars core, subject to an initial temperature distribution given by the profiles in Figure 7. We assume that, during the 500 Myr prior to the giant impact sequence, the thermal evolution of Mars had established a core with an adiabatic temperature distribution and a convecting mantle,

with surface and basal thermal boundary layers where heat transferred largely by conduction and an interior with a nearly adiabatic temperature distribution. The impact-induced temperature changes in the lower mantle are rather small compared

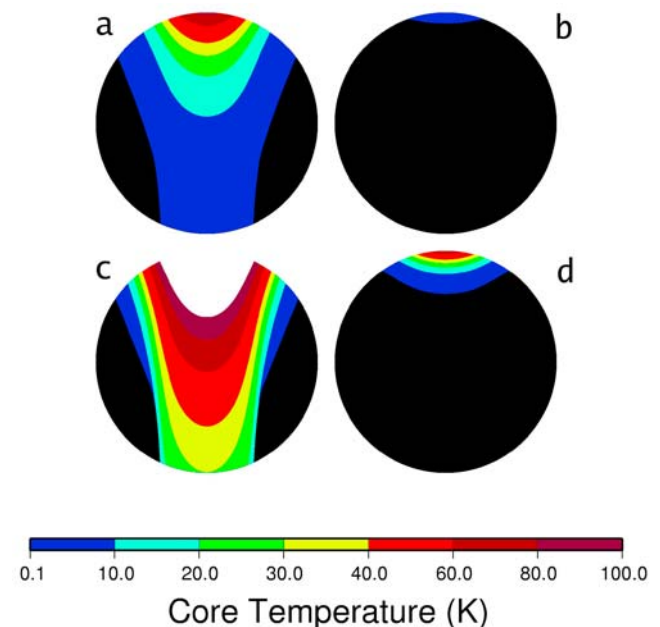


**Figure 6.** Temperature increase in the core by direct shock wave heating, enlarged from Figure 2 for better illustration. The temperature in the white area in Figure 6c is higher than the saturation temperature of 100 K. See Figure 2 for details.

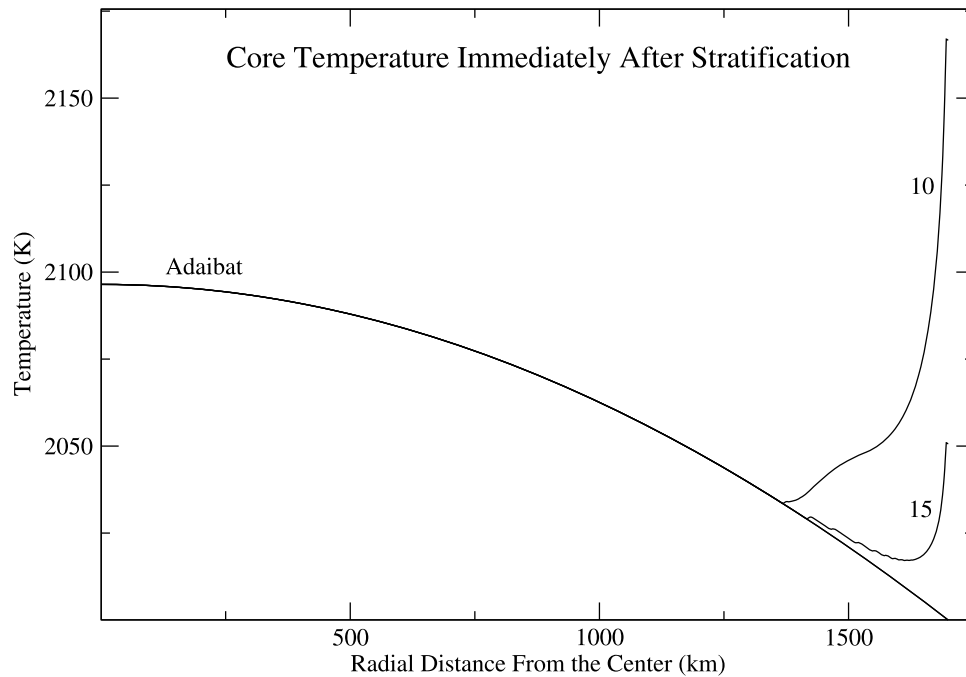


**Figure 7.** The spherically symmetric temperature distribution in the core immediately after stratification. The temperature increase due to shock wave is added to the preimpact adiabatic temperature that starts at 2000 K at the core-mantle boundary. The numbers on the curves denote the impact velocity in km/s.

to the preexisting temperature variation across its basal thermal boundary layer so that the dynamics of the mantle are not much affected by the temperature changes near the core-mantle boundary due to subsequent core cooling during the destratification of the core. In contrast, the dynamics of the core are greatly affected by the temperature changes in this region, because the thermal stratification event concentrates the impact heat in the outer parts of the core.

[32] Figure 7 shows that the outer part of the stratified core does not convect immediately after the stratification because the temperature gradient is positive there. Similarly, the lower part of the core does not convect either, because it is overlain by the higher-temperature outer part. Heat transfer in the core immediately after the stratification is therefore by thermal conduction. However, because of the very low viscosity of the liquid iron, penetrative convection develops below the core-mantle boundary in a relatively short time. Figure 8 shows the temperature distribution in the core and the overlying thermal boundary layer of the mantle schematically during destratification, including a penetrative convective layer below the core-mantle boundary, with conduction deeper in the core. While the impact heat is being exhausted to the mantle, the middle part of the core heats, by conduction from the outer part and partly by upward heat conduction along the adiabat from the central part.

[33] The heat flux out of the core during the destratification phase is primarily controlled by the lower thermal boundary layer of the mantle, which is also perturbed by shock heating. This perturbation as it affects the heat flow at the core-mantle boundary is small. Figure 9 shows the impact temperature increase at the base of the mantle versus the colatitude relative to the subimpact point. Shock waves heat the base of the mantle up to  $\sim 54^\circ$  colatitude, equivalent to  $\sim 21\%$  of the

surface of the core, and major shock heating occurs over  $\sim 10\%$  of the surface. The temperature distribution across the lower thermal boundary layer of mantle overlying 79% of the core is not affected by the impact at all. Subsequent cooling of the core is dominated by the heat loss through this part of the boundary to the mantle. This slightly overestimates the rate of core cooling because the effect of the impact heated part of the lower thermal boundary layer of the mantle is ignored.

[34] We consider the thermal interaction of the core and the overlying thermal boundary layer of the mantle subsequent to the core stratification event. The mantle boundary layer is assumed to be 100 km thick with a linear temperature distribution before the impact. The temperature gradient in the mantle boundary layer corresponds to a heat flux of 15 mW/m<sup>2</sup>, which is comparable to the heat flux estimated at about 4 Ga according to stagnant lid thermal evolution models of Mars [Breuer and Spohn, 2003; Williams and Nimmo, 2004; Arkani-Hamed, 2005b; Roberts et al., 2009].

[35] The temperature  $T$  in the conductive regions of the core and in the thermal boundary layer of the mantle is calculated by solving the conduction equation,

$$\partial T / \partial t = (1/r^2) \partial (r^2 \kappa \partial T / \partial r) / \partial r, \quad (14)$$

where  $t$  is time,  $r$  is the distance from the center, and  $\kappa$  is the thermal diffusivity. The boundary condition at the center of the core is zero heat flux. At the interface between the conducting and convecting regions, we enforce the continuity of temperature and heat flux. At the top of the mantle thermal boundary layer, we fix the temperature at its preimpact value. In the penetrative convection zone of the core, there are two very thin thermal boundary layers, one at the top and the other at the bottom of the zone.

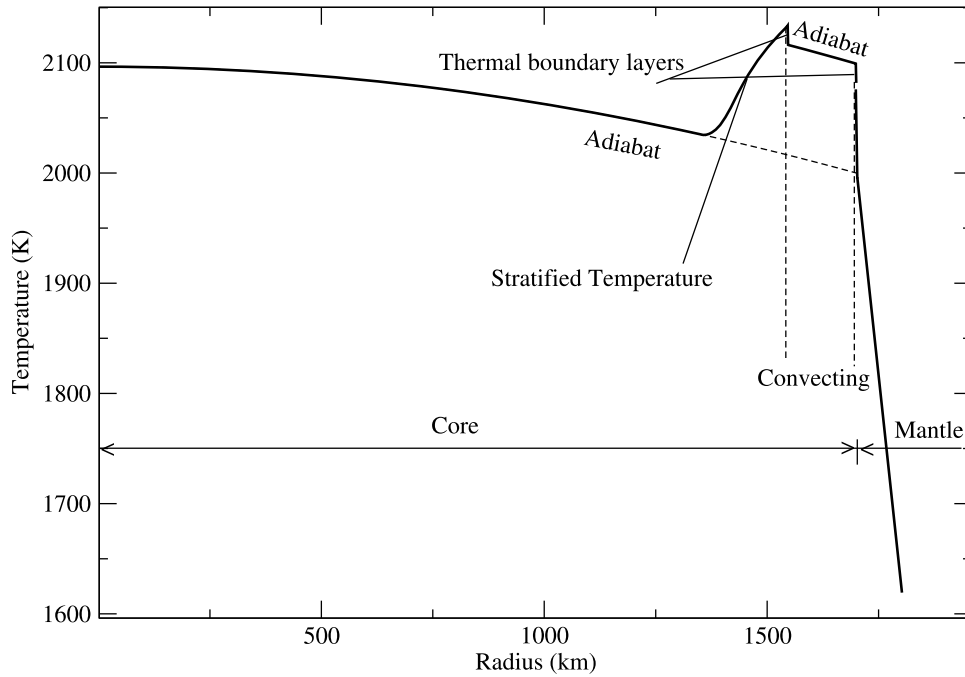


**Figure 8.** Schematic diagram of the temperature distribution in the core and the lower thermal boundary layer of the mantle some time after the stratification. The excess impact heat in the upper parts of the core is largely transmitted to the mantle by convection and partly to the inner parts by conduction. An adiabatic temperature prevails in the convecting part.

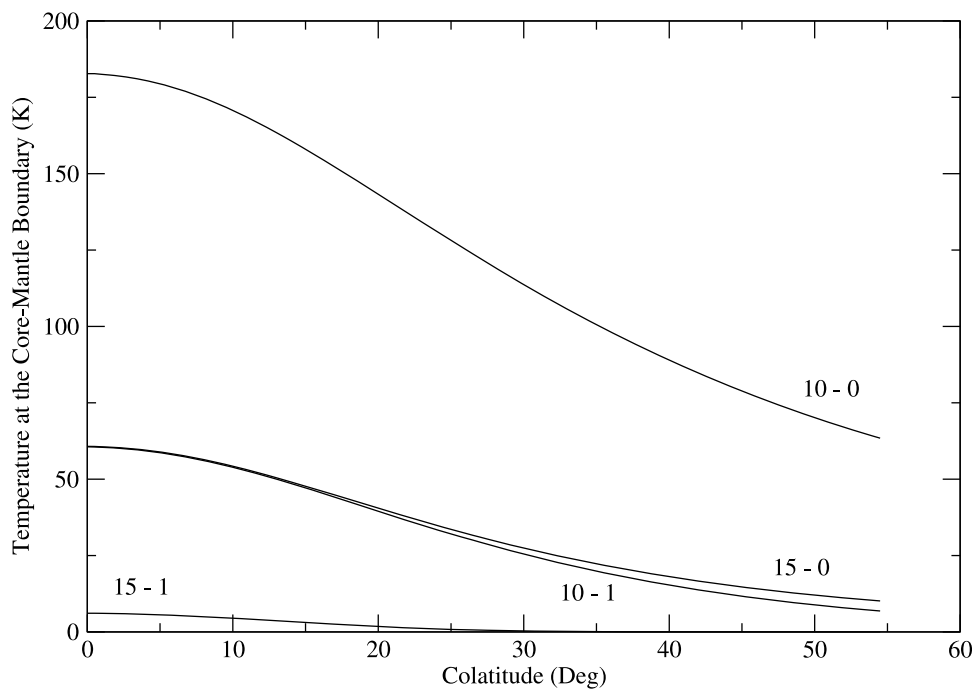


**Figure 9.** Impact-induced temperature increase at the base of the mantle immediately above the core versus colatitude relative to the impact point. The first number on a curve denotes the impact velocity in km/s, and the second number is the shock heating model, 0 = “ordinary” and 1 = “foundering.”

[36] The temperature in the penetrative convection zone is determined by solving the following enthalpy equation,

$$4\pi R_1^2 q_1 = 4\pi R_c^2 q_c + \int 4\pi r^2 dr C_{pc} \rho_c \partial T / \partial t, \quad (15)$$

where  $R_1$  is the radius of the bottom of the penetrative convection zone,  $R_c$  is the core radius,  $q_1$  and  $q_c$  are heat fluxes at  $R_1$  and  $R_c$ , respectively,  $C_{pc}$  is the specific heat of the core at constant pressure, and  $\rho_c$  is the core density. The integral is evaluated throughout the penetrative convection zone, which includes the two thermal boundary layers where temperature changes linearly, and a bulk convecting region, where an adiabatic temperature distribution is assumed.

[37] The thermal boundary layer thickness  $\delta$  of the convecting zone, assumed identical for both top and bottom layers, is determined following *King et al.* [2009] and using

$$\delta = 0.5d / Nu, \quad (16)$$

where the Nusselt number  $Nu$  is related to the Rayleigh number of the convection  $Ra$  by

$$Nu = 0.16Ra^{2/7}, Ra > Ra_t (\text{non-rotating convection}) \quad (17a)$$

or, alternatively,

$$Nu = (Ra/Ra_c)^{6/5}, Ra < Ra_t (\text{rotating convection}) \quad (17b)$$

depending on the Rayleigh number of the convecting zone at a given time. The Rayleigh number  $Ra$  is defined as

$$Ra = g_c \alpha \Delta T' d^3 / \kappa \nu, \quad (18)$$

where  $d (= R_c - R_1)$  is the total thickness of the convecting zone,  $g_c$  is the gravitational acceleration at the core-mantle boundary,  $\alpha$  is the thermal expansion coefficient,  $\Delta T'$  is the potential temperature drop from the bottom to the top of the convecting zone calculated relative to the prevailing adiabatic temperature in the convecting zone,  $\kappa$  is the thermal diffusivity, and  $\nu$  is the kinematic viscosity of the liquid iron core. See Table 1 for parameter values. The critical Rayleigh number for onset of convection  $Ra_c$  is defined by

$$Ra_c = 6E^{-4/3}, \quad (19)$$

where  $E$  is the Ekman number,

$$E = \nu / 2\Omega d^2, \quad (20)$$

and  $\Omega$  is the angular velocity of the rotation of Mars, calculated assuming a rotation period of 24 h. The transition Rayleigh number  $Ra_t$  that separates strong from weak rotational influence is determined in terms of the critical Rayleigh number by equating the two expressions (17a) and (17b). For  $Ra < Ra_t$ , the rotation of the core hampers vertical motion and reduces the heat transfer across the convecting zone, whereas the rotation has minor effects on the heat transfer when  $Ra > Ra_t$ . The factor 0.5 is introduced in (16) because there are two thermal boundary layers in the convecting zone whereas the  $\Delta T'$  appearing in the definition of the Rayleigh number (18) denotes the total temperature drop across the convecting zone as mentioned above.

[38] The thermal boundary layers of the convecting zone of the core are included in solving the heat conduction equation in the thermal boundary layer of the mantle and in the deeper conducting part of the core. However, the thickness of the layers is very small compared to the grid interval of 1 km used for solving the conduction equation. For simplicity in computation, we keep using the constant grid interval of 1 km but increase the thermal diffusivity in the boundary layers by a factor of  $\Delta r / \delta$  to assure the accurate heat fluxes through the boundary layers of the core. Because  $\delta$  is a time varying function in the penetrating convection considered, the modified thermal diffusivity of the boundary layers and the time step  $\Delta t$  used in solving the conduction equation are also time dependent.  $\Delta t$  is determined at the beginning of each time step such that heat diffuses by less than  $\delta/2$  during that time step. Detailed numerical procedures are presented in Appendix A.

[39] Figures 10a and 10b show the spherically symmetric temperature distribution in the core and the overlying thermal boundary layer of the mantle at certain times after the core stratification, assuming that Utopia impact occurred at 10 or 15 km/s and that the kinematic viscosity of the core is  $\nu = 10^{-4}$  m<sup>2</sup>/s, which is within the viscosity values suggested for the outer core of the Earth [*Secco*, 1995]. We have also used viscosity values of  $\nu = 10^{-2}$ , 1, 10<sup>2</sup>, and 10<sup>4</sup> m<sup>2</sup>/s, and the results are almost identical to those presented in these figures. Figure 11 shows the time variations of the thickness of the penetrative convection zone corresponding to the viscosity values and the two impact velocities. The thermal evolution results are almost identical, emphasizing that the thermal evolution of the core is mainly controlled by the mantle, rather than the viscosity of the core, at least within the viscosity values considered.

[40] According to the results in Figure 11, it takes about 130 million years for the core to exhaust the impact heat when the impact velocity is 10 km/s but only about 24 million years when the impact velocity is 15 km/s. While impact heat is being exhausted to the mantle, heat is conducted from the central part of the core to its middle part because of the negative gradient of the adiabatic temperature. This reduces the temperature gradient below the adiabat in the deeper part of the core and tends to further inhibit thermal convection there. However, shortly after the exhaustion of the impact heat, the upper convection zone penetrates very rapidly to the center of the core and global convection in the core resumes. This rapid penetration is due to the fact that the temperature in the deeper parts of the core remains close to the adiabatic temperature as seen in Figures 10a and 10b. The rapid penetration increases the characteristic length of convection by a factor of  $\sim 3$  and the thermal Rayleigh number  $Ra$  ( $\sim d^3$ ) by a factor of  $\sim 27$ , which is 2 orders of magnitude higher than the required increase for initiation of core dynamo as indicated by the numerical simulation models of *Kuang et al.* [2008].

## 6. Discussion and Conclusions

[41] We investigated the effects of Utopia impact, the largest of the 20 impacts occurred on Mars at about 4 Ga, on the thermal evolution of Mars core. We calculated the impact heating using the average model of *Pierazzo et al.* [1997] for the shock wave pressure distribution, the ‘‘ordinary’’ and ‘‘foundering’’ shock heating models of *Watters et al.* [2009]

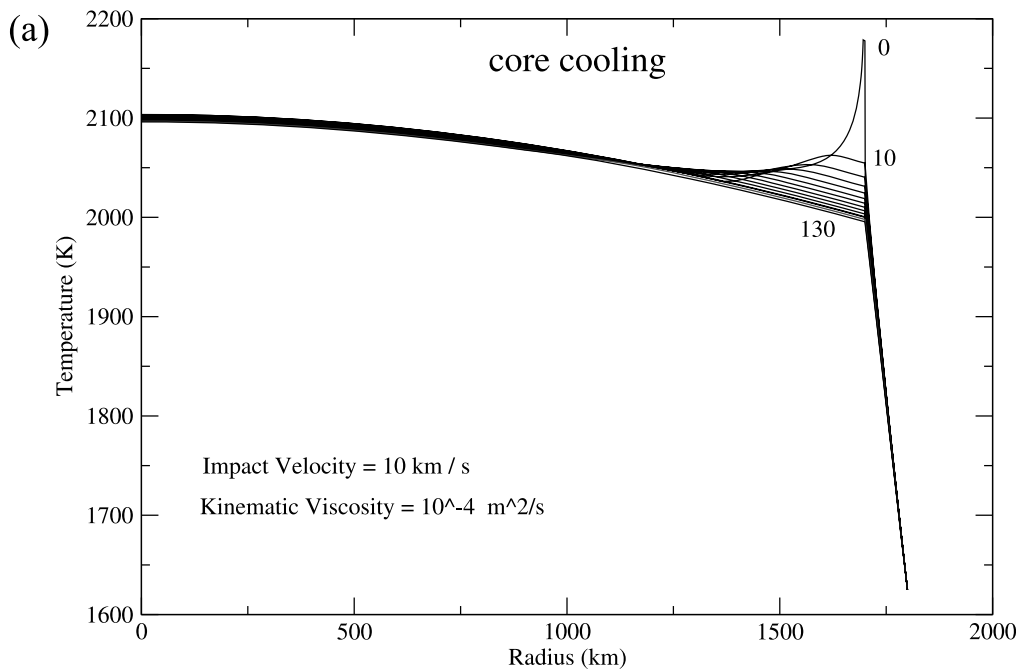


**Figure 10.** (a) Spherically symmetric temperature distribution in the core for the model with an impact velocity of 10 km/s. The numbers on the curves denote time after the impact in Myr. It takes about 130 Myr for the core to exhaust the excess heat due to the impact. (b) The same as Figure 10a but for an impact velocity of 15 km/s. Note that the excess heat of impact is much less in this case due to faster decay of shock pressure outside the isobaric sphere. The numbers on the curves denote time after the impact in Myr. It takes no more than 24 Myr for the core to exhaust the excess heat.

and assuming impact velocities of 10 and 15 km/s. We examined the impact heating effects on the deeper parts of the mantle and the core. Three stages with vastly different characteristic times were investigated: the first stage was the shock wave propagation and heating of Mars that occurred within minutes following impact, the second stage was the core stratification that took about a few tens of years, and the third stage was the core cooling that lasted for tens of millions of years. We found that the impact heating of the deeper parts of the mantle does not significantly reduce the heat flux at the core-mantle boundary. For the Utopia impact, the reduction is probably too small to stop convection even if the core was in a subcritical state at the impact time. The amount of direct heating of the core depends on the nature of the shock wave. According to the “ordinary” shock heating model, the Utopia impact was capable of heating the core significantly by the direct propagation of the shock wave in the core, but according to the “foundering” model, only a localized region in the uppermost part of the core directly beneath the impact site was heated. In either case, however, the impact-heated core becomes thermally stratified in the upper 300–400 km. This stratification suppresses preimpact thermal convection in the core and would therefore diminish a thermally driven core dynamo on the time scale of free decay of the dipole magnetic field,  $\sim 15$  kyr [Arkani-Hamed and Olson, 2010].

[42] The removal of the heat concentrated below the core-mantle boundary occurs by conduction to the mantle and conduction into the deeper part of the core. If the heat flow into the mantle is sufficient, penetrative convection develops in a layer beneath the core-mantle boundary. Because of the initially strong stratification, the penetrative convection layer

thickens slowly at first but grows very rapidly once the strong stratification is removed and adiabatic temperature distribution prevails over the entire core. This rapid growth of the penetrative convection layer increases the thermal Rayleigh number of the core, in principle, allowing the core to regenerate a convective dynamo. For a low Utopia impact velocity of 10 km/s, the destratification process may require  $\sim 130$  Myr after basin formation, but only 24 Myr for the same impact with a velocity of 15 km/s.

[43] The results presented above are based on several assumptions, some of which are optimistic and some conservative. The important assumptions are briefly discussed below.

### 6.1. Shock Heating Models

[44] From the three shock heating models “ordinary,” “climbing,” and “foundering” [Watters *et al.*, 2009], we considered the first which yields the largest impact heating, and the last which produces the least. The “ordinary” model does not take into account a very important factor, the effect of the preexisting lithostatic pressure, and greatly overestimates the amount of shock heating specially near the base of the mantle (W. Watters, 2009, personal communication). The “foundering” model does not account for the effect of increasing density with depth in the mantle of a realistic internal model of Mars and the corresponding changes in the Hugoniot as the pressure and density increase with depth. Although these effects are incorporated in the “climbing” model, the temperature increase in the lower parts of the mantle calculated by this model is within only 15 K of the “foundering” model [see Watters *et al.*, 2009, Figure S17].

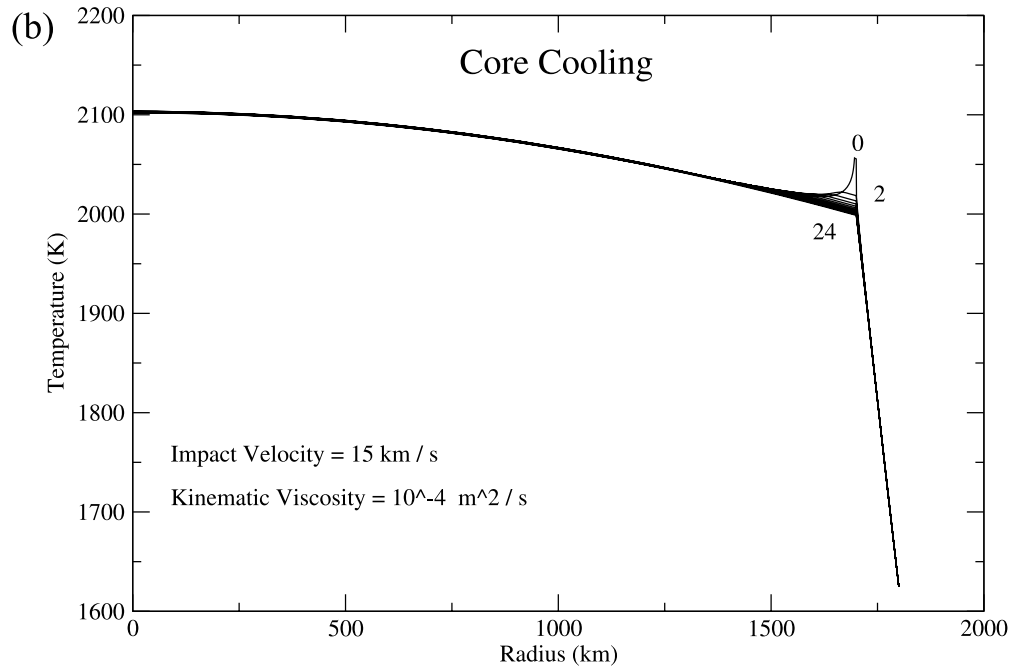


**Figure 10.** (continued)

The difference would be even less for the two-layered internal model of Mars adopted in the present study. We regard the “foundering” model more realistic than the “ordinary” model, but very close to the “climbing model.”

[45] It is important to emphasize that the “foundering” models shown in Figure 6 do not heat the core appreciably. The foundering model corresponding to an impact velocity of 10 km/s stratifies a very small portion of the core, and the impact heat can be exhausted in less than 3 Myr. That foundering model corresponding to the impact velocity of 15 km/s heats the core even less and does not cause appreciable stratification.

## 6.2. Basin Scaling Laws

[46] The scaling laws given by equations (1) and (2), although standard, have been questioned for the large impact that created Utopia basin [Frey, 2008], and their predictions must therefore be regarded as rough estimates. It is possible, for example, that postimpact collapse of a large impact basin is controlled by dynamic weakening along impact-induced faults [e.g., Senft and Stewart, 2009], and the final diameter of the basin is much closer to its transient diameter than that calculated from equation (1). Roberts *et al.* [2009] examined the possibility that the final basin diameter was the same as the transient diameter, an extreme case, as emphasized by the authors. We calculated the impact heating by this extreme case scenario for impact velocities of 10 and 15 km/s, adopting the “foundering” shock heating model. The resulting impact heating in the base of the mantle is capable of reducing the heat flux out of the core by about 1%, indicating that this highly optimistic scenario model could marginally suppress the thermally driven core dynamo even if the convection happens to be at subcritical state with a large solid inner core of 500 km [Kuang *et al.*, 2008]. As mentioned

before, however, a solid inner core is not predicted by the successful stagnant lid convection models. This level of impact heating of the mantle would have negligible effects on supercritical core convection. In contrast, the direct heating of the core in this same scenario would thermally stratify the core and extinguish a convective dynamo in a short time. For the impact velocity of 10 km/s, it takes about 55 Myr for the stratified core to exhaust its impact heat and possibly regenerate a core dynamo, but only about 20 Myr for the impact velocity of 15 km/s.

## 6.3. Shock Pressure Model

[47] Figure 12 shows the normalized shock wave pressure outside the isobaric sphere as a function of distance  $r$  from the center of the sphere for impact velocities of 15 and 10 km/s according to the model proposed by Melosh [1989],

$$P_s(r) = \rho_0 u_0 \left[ C + S u_0 (r_c/r)^{1.87} \right] (r_c/r)^{1.87}, \quad (21)$$

the average model of Pierazzo *et al.* [1997], equation (3b), and the model proposed by Mitani [2003], for which

$$\begin{aligned} P_s(r) &= P_s(r_c) (r_c/r)^n; \\ n &= 1.2 \text{ for } P_s < P_H, \\ n &= 2.5 \text{ for } P_H < P_s < 10P_s, \text{ and} \\ n &= 1.2 \text{ for } P > 10P_s, \end{aligned}$$

where  $P_H$  (= 5 GPa) is the Hugoniot elastic limit pressure. The pressure from Mitani’s model lies between the two other models. The average Pierazzo *et al.* [1997] model adopted in this study is the most optimistic with slowly decaying shock pressure with depth compared to Melosh’s and Mitani’s models. This is specially the case near the core-mantle boundary where the other models predict 2–10 times less

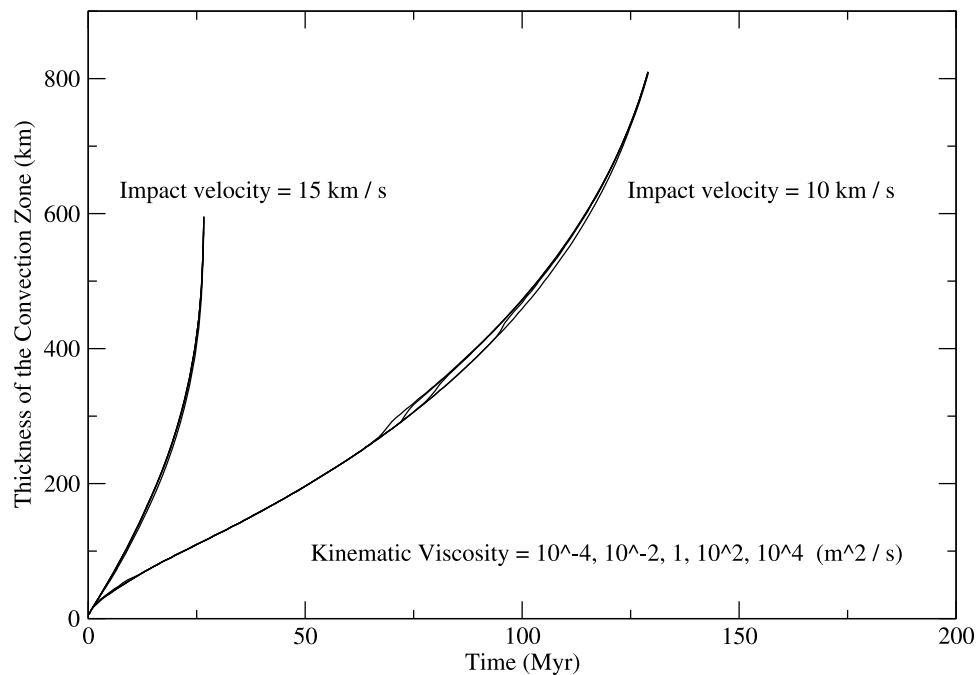


**Figure 11.** Thickness of the convecting layer in the upper part of the core as a function of time after the stratification of the core. Note that changing the viscosity of the liquid outer part by 8 orders of magnitude has little effect on the thermal evolution of the core. The core cooling is mainly controlled by the mantle.

pressure, implying that the impact-induced temperature perturbations presented above (Figure 2) are somewhat overestimated.

#### 6.4. Pre-existing Mantle Convection

[48] Figure 2 shows the temperature increase due to impact heating. No attempt is made to calculate the effect of the preexisting temperature distribution in the mantle on our shock heating functions. This is partly because this has already been done by other investigators [see *Roberts et al.*, 2009; *Watters et al.*, 2009], but also because we wish to isolate the impact heating effect. The preimpact thermal convection in the mantle most likely had established two thermal boundary layers, one at the surface and the other near the core-mantle boundary, where heat transfer was mainly by conduction and temperature changed rapidly in the radial direction. The assumption of linearity in heat conduction allows us to directly compare the heat flux shown in Figure 3 to the heat flux out of the core calculated on the basis of a preexisting thermal boundary layer in order to estimate the impact effects on the heat flux out of the core. The preimpact temperature in the main part of the convecting mantle was likely close to an adiabatic temperature plus/minus a few hundred K lateral variations among the upwelling and downgoing circulations. The impact induced temperature increase was well over 1000 K in the upper 600 km, which resulted in a huge amount of melting and evaporation causing massive volcanism and upwelling along the entire column of the mantle directly beneath the impact site to fill the vacuum created by the outpouring of the molten material. The observed surface topography and gravity field over Utopia basin require excess density of about  $140 \text{ kg/m}^3$  within a 50 km thick layer over the entire area of the basin [see *Arkani-*

*Hamed and Riendler*, 2002, Figure 1c], which is equivalent to  $\sim 6.3 \times 10^{19} \text{ kg}$  of excess mass.

[49] Here we offer some reasonable conjectures about the longer term adjustment of the mantle to its shock heating and how that might have affected the core. It is expected that the greatly enhanced buoyancy of the partially molten material remaining in the isobaric region, with its high temperature and the retention of low-density melt, initiated a mega plume of partially molten mantle that ascended at a high velocity, as demonstrated by *Ghods and Arkani-Hamed* [2007] for the impact on the Moon that created the giant Aitken basin (see also the abstract by *Ghods and Arkani-Hamed* [2008] for Mars impacts). We note that the buoyancy enhancement by retention of only 3% melt (with a density of  $2700 \text{ kg/m}^3$ ) is equivalent to that due to temperature increase of about 300 K, assuming thermal expansion coefficient of  $3 \times 10^{-5}$  for the mantle material. The rapid upwelling of the plume is expected to have elevated the impact-heated mantle material above from the core-mantle boundary and caused appreciable lateral motion in the base of the mantle, with replacement of the impact-heated material by the colder, unshocked material from the surrounding mantle. With this sequence of events, the reduction of the heat flux at the core-mantle boundary due to the impact heating of the mantle is expected to be very short lived, and the preimpact temperature distribution in the thermal boundary layer of the mantle would have prevailed very rapidly.

[50] The above discussion highlights the uncertainties in applying the model results presented in this paper to events in early Mars history. The actual relationship between the transient and final diameters of a giant basin, as well as the heating mechanism of the mantle and core by the shock wave, may lie somewhere between those explored in this study. Nevertheless, based on the best available models for shock

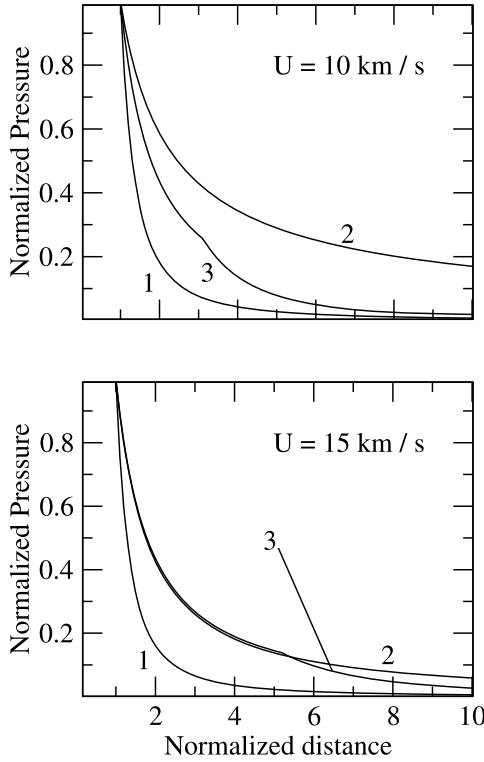


**Figure 12.** Decay of the shock wave pressure versus distance from the center of the isobaric sphere. The pressure is normalized to that in the isobaric sphere and the distance is normalized to the radius of the isobaric sphere.  $U$  is the impact velocity. The numbers on the curves denote the shock pressure models: 1, *Melosh* [1989]; 2, the average model of *Pierazzo et al.* [1997]; and 3, *Mitani* [2003]. The core-mantle boundary is at the normalized distance of  $\sim 7.5$ .

heating, we conclude that the direct heating of Mars core by the Utopia impact had a larger effect than the indirect thermal effects on the core from shock heating in the mantle.

[51] It is perhaps worth emphasizing that investigations into the possible relationships between giant impacts and the history of the Martian dynamo are just beginning, and there is much to be learned. For example, it is not certain that a causal relationship actually existed between these two events or whether they were simply coincidental in time. No attempt is made in this study to tailor a model or a suite of models just to reconcile the two events. We hope that our results together with those of others cited in this paper provide good incentive to further investigate this issue, in the light of new observations and more realistic, better constrained models.

### Appendix A: Numerical Simulation of Penetrative Convection

[52] This appendix provides a brief description of the numerical technique used to simulate penetrative convection in the outer convecting part of the core during the thermal evolution of a stratified liquid core that is overlain by a solid lower thermal boundary layer of the mantle. No radioactive heat sources are considered. The domain of integration includes the entire core and the overlying thermal boundary layer, assumed to be 100 km thick. At a given time in the

evolution, the domain is subdivided into three parts, a conducting deeper core to a radius of  $R_1$ , the convecting out core between  $R_1$  and the core radius  $R_c$  ( $= 1700$  km) and a conducting mantle to a radius of  $R_2$  ( $= 1800$  km). Because the convecting part penetrates to deeper parts of the core,  $R_1$  is time dependent. The convective part is also subdivided into three sublayers, the lower and the upper thermal boundary layers where heat is transferred by conduction and the middle convecting layer where heat is transferred by convection. The two thermal boundary layers of the core are assumed to have identical thicknesses since the entire convecting layer is always thin. The thickness of a thermal boundary layers  $\delta$  is time dependent because the thickness of the entire convecting layer  $d$  ( $= R_c - R_1$ ), increases in time and  $\delta$  depends on  $d$ .

[53] The heat conduction equation (14) is expressed numerically using the central difference technique, which reduces the equation to

$$\beta_{i-1/2}T_{i-1} + (\beta_{i-1/2} + \beta_{i+1/2} + 1)T_i + \beta_{i+1/2}T_{i+1}\}_{(t+\Delta t)} = \{T_i\}_t, \quad (\text{A1})$$

where

$$\beta_{i-/+1/2} = (\kappa_i \Delta t / \Delta r^2) (r_{i-/+1/2} / r_i)^2 \quad (\text{A2})$$

and the index  $i$  refers to  $r = r_i$ , where  $r$  is the distance from the center,  $T$  is temperature,  $t$  is time, and  $\kappa$  is the thermal diffusivity. The temperature on the left-hand side is at time  $t + \Delta t$  and that on the right-hand side is at time  $t$ . The time interval  $\Delta t$  is determined at the beginning of each time step using the stability criterion,

$$\Delta t = \delta^2 / 4\kappa, \quad (\text{A3})$$

assuring that heat does not diffuse by more than  $\delta/2$  during that interval. Equation (A1) is solved in the conducting deeper part of the core plus the lower thermal boundary of the core,  $0 < r < R_1 + \delta$ , and in the mantle layer plus the upper thermal boundary of the core,  $R_c - \delta < r < R_2$ . The thickness of a thermal boundary layer of the core is determined on the basis of equations (16)–(20). For numerical simplicity, we adopt a constant grid interval of  $\Delta r = 1$  km throughout the entire domain of integration. However, because of very low viscosity of the liquid core (we examined kinematic viscosities ranging from  $10^{-4}$  to  $10^4$  m<sup>2</sup>/s)  $\delta < \Delta r$ . To compensate for this difference and assure that heat transfer through the thermal boundary layers of the core is not affected by the gridding, the thermal diffusivity of the thermal boundary layers is increased by a factor of  $\Delta r / \delta$ , which in turn makes the diffusivity time dependent.

[54] For solving the enthalpy equation (15) in the convecting part of the core, the temperature distribution in the thermal boundary layers is assumed linear with a time-varying slope. The adiabatic temperature at a given point  $r_j$  in the convecting interior  $T_{rj}$  is related to the temperature at the base of the upper thermal boundary layer  $T_{(R_c - \delta)}$  of the convecting zone by

$$T_{rj} = T_{(R_c - \delta)} \exp\left\{2\pi\rho_c\alpha_c G \left[ (R_c - \delta)^2 - r_j^2 \right] / 3 C_{pc} \right\}, \quad (\text{A4})$$

where  $G$  is the gravitational constant and the core is assumed to have uniform density. This reduces the enthalpy equation to

$$\zeta_1 T_{R_1} + \zeta_2 T_{(R_c-\delta)} + \zeta_3 T_{R_c} = \xi, \quad (\text{A5})$$

where the coefficients  $\zeta_1$ ,  $\zeta_2$ , and  $\zeta_3$ , and the right-hand side  $\xi$  are functions of the physical and geometrical parameters. They are evaluated at time  $t$ , but  $T_{R_1}$ ,  $T_{(R_c-\delta)}$ , and  $T_{R_c}$  are calculated at time  $t + \Delta t$ .

[55] Equations (A1) and (A5) are combined into a single  $L \times L$  three-diagonal matrix equation using the continuity of the temperature and heat flux at the boundaries of the convecting zone,

$$M_1 T_{i-1} + M_2 T_i + M_3 T_{i+1} = N_i, \quad (\text{A6})$$

where  $i$  runs from 1 corresponding to 1 km distance from the center to  $J$  corresponding to the distance  $R_1$  from the center to cover the conducting part of the core.  $i = J + 1$  stands for the distance  $R_c - \delta$  from the center, and  $i$  again runs from  $J + 2$ , the core-mantle boundary, to  $L$  the top of the mantle layer.  $M_1$ ,  $M_2$ ,  $M_3$ , and  $N$  denote the corresponding terms in equations (A1) and (A5). The boundary conditions for equation (A6) are isothermal within a central sphere of 1 km radius [ $T_1 = T$  (at 0 km)] and fixed temperature  $T_m$  at the top of the mantle layer [ $T_{(L+1)} = T_m$ ]. The latter is determined immediately before the impact assuming a linear temperature distribution in the layer corresponding to a heat flux of  $15 \text{ mW/m}^2$  at the core-mantle boundary.

[56] We note that  $L$  is time dependent because of the penetrating nature of the convection zone in the core. The base of the convecting zone is determined at each time step by inspecting the slope of the temperature profile marching from the center outward. The base of the convecting zone is identified where the slope becomes equal to or smaller than the slope of the corresponding adiabatic temperature distribution.

[57] **Acknowledgments.** This research is partly supported by Natural Sciences and Engineering Research Council (NSERC) of Canada to J.A.H. and partly by grant EAR-0604974 from the U. S. National Science Foundation to P.O. We would like to thank W. Watters at Cornell University for the discussions we had in the early stages of this study.

## References

Acuña, M. H., et al. (1999), Global distribution of crustal magnetization discovered by the Mars Global Surveyor MAG/ER experiment, *Science*, *284*, 790–793.

Aki, K., and P. G. Richards (2002), *Quantitative Seismology*, 2nd ed., University Science Books, Sausalito, Calif.

Antretter, M., M. Fuller, E. Scott, M. Jackson, B. Moskowicz, and P. Solheid (2003), Paleomagnetic record of Martian meteorite ALH84001, *J. Geophys. Res.*, *108*(E6), 5049, doi:10.1029/2002JE001979.

Arkani-Hamed, J. (2004), Timing of the Martian core dynamo, *J. Geophys. Res.*, *109*, E03006, doi:10.1029/2003JE002195.

Arkani-Hamed, J. (2005a), On the possibility of single-domain/pseudosingle-domain magnetic particles existing in the lower crust of Mars: Source of the strong magnetic anomalies, *J. Geophys. Res.*, *110*, E12009, doi:10.1029/2005JE002535.

Arkani-Hamed, J. (2005b), Magnetic crust of Mars, *J. Geophys. Res.*, *110*, E08005, doi:10.1029/2004JE002397.

Arkani-Hamed, J. (2009), Did tidal deformation power the core dynamo of Mars?, *Icarus*, *201*, 31–43.

Arkani-Hamed, J., and L. Riendler (2002), Stress differences in the Martian lithosphere: Constraints on the thermal state of Mars, *J. Geophys. Res.*, *107*(E12), 5119, doi:10.1029/2002JE001851.

Arkani-Hamed, J., and P. Olson (2010), Giant impact stratification of the Martian core, *Geophys. Res. Lett.*, *37*, L02201, doi:10.1029/2009GL041417.

Arkani-Hamed, J., B. Seyed-Mahmoud, K. D. Aldridge, and R. E. Baker (2008), Tidal excitation of elliptical instability in the Martian core: Possible mechanism for generating the core dynamo, *J. Geophys. Res.*, *113*, E06003, doi:10.1029/2007JE002982.

Bjorkman, M. D., and K. A. Holsapple (1987), Velocity scaling impact melt volume, *Int. J. Eng.*, *5*, 155–163.

Breuer, D., and T. Spohn (2003), Early plate tectonics versus single-plate tectonics on Mars: Evidence from magnetic field history and crust evolution, *J. Geophys. Res.*, *108*(E7), 5072, doi:10.1029/2002JE001999.

Christensen, U. R., and J. Wicht (2007), Numerical dynamo simulations, in *Treatise on Geophysics*, edited by P. Olson, vol. 8, pp. 245–282, Elsevier.

Frey, H. (2008), Ages of very large impact basins on Mars: Implications for the late heavy bombardment in the inner solar system, *Geophys. Res. Lett.*, *35*, L13203, doi:10.1029/2008GL033515.

Frey, H. V., J. H. Roark, K. M. Shockey, E. L. Frey, and S. E. H. Sakimoto (2002), Ancient lowlands on Mars, *Geophys. Res. Lett.*, *29*(10), 1384, doi:10.1029/2001GL013832.

Ghods, A., and J. Arkani-Hamed (2007), Impact-induced convection as the main mechanism for formation of lunar mare basalts, *J. Geophys. Res.*, *112*, E03005, doi:10.1029/2006JE002709.

Ghods, A., and J. Arkani-Hamed (2008), Impact-induced melting of the martian mantle, *Eos Trans. AGU*, *89*(53), Fall Meet. Suppl., Abstract P33B-1452.

Gubbins, D., T. G. Masters, and J. A. Jacobs (1979), Thermal evolution of the Earth's core, *Geophys. J. R. Astron. Soc.*, *59*, 57–99.

Han, Z., and X. Yin (1993), *Shock Dynamics*, Kluwer Acad., Dordrecht/Boston/London.

Hauck, S. A., II, and R. J. Phillips (2002), Thermal and crustal evolution of Mars, *J. Geophys. Res.*, *107*(E7), 5052, doi:10.1029/2001JE001801.

Holsapple, K. A. (1993), The scaling of impact processes in planetary sciences, *Annu. Rev. Earth Planet. Sci.*, *21*, 333–373.

Johnson, C. L., and R. J. Phillips (2005), Evolution of the Tharsis region of Mars: Insights from magnetic field observations, *Earth Planet. Sci. Lett.*, *230*, 241–254.

King, E. M., S. Stellmach, J. Noir, U. Hansen and J. M. Aurnou (2009), Boundary layer control of rotating convection systems, *Nature*, *457*, doi:10.1038/nature07647.

Kuang, W., W. Jiang, and T. Wang (2008), Sudden termination of Martian dynamo?: Implications from subcritical dynamo simulations, *Geophys. Res. Lett.*, *35*, L14204, doi:10.1029/2008GL034183.

Lillis, R. J., H. V. Frey, and M. Manga (2008), Rapid decrease in Martian crustal magnetization in the Noachian era: Implications for the dynamo and climate of early Mars, *Geophys. Res. Lett.*, *35*, L14203, doi:10.1029/2008GL034338.

Louzada, K. L., and S. T. Stewart (2009), Effects of planet curvature and crust on the shock pressure field around impact basins, *Geophys. Res. Lett.*, *36*, L15203, doi:10.1029/2009GL037869.

Melosh, H. J. (1989), *Impact Cratering: A Geologic Process*, Oxford Univ. Press, New York.

Mitani, N. K. (2003), Numerical simulations of shock attenuation in solids and reevaluation of scaling law, *J. Geophys. Res.*, *108*(E1), 5003, doi:10.1029/2000JE001472.

Neukum, G., and D. V. Wise (1976), Mars: A standard crater curve and possible new time scale, *Science*, *194*, 1381–1387.

Nimmo, F., and D. J. Stevenson (2000), Influence of early plate tectonics on the thermal evolution and magnetic field of Mars, *J. Geophys. Res.*, *105*, 11,969–11,979.

Pierazzo, E., A. M. Vickery, and H. J. Melosh (1997), A reevaluation of impact melt production, *Icarus*, *127*, 408–423.

Pruis, M. J., and K. L. Tanaka (1995), The Martian Northern Plains did not result from plate tectonics: Houston, Texas, Lunar and Planetary Institute, *Lunar Planet. Sci.*, *XXVI*, 1147.

Roberts, J. H., R. J. Lillis, and M. Manga (2009), Giant impacts on early Mars and the cessation of the Martian dynamo, *J. Geophys. Res.*, *114*, E04009, doi:10.1029/2008JE003287.

Schubert, G., S. C. Solomon, D. L. Turcotte, M. J. Drake, and N. H. Sleep (1992), Origin and thermal evolution of Mars, in *Mars*, edited by H. H. Kieffer et al., pp. 147–183, Univ. of Ariz. Press, Tucson.

Schubert, G., C. T. Russell, and W. B. Moore (2000), Timing of the Martian dynamo, *Nature*, *408*, 666–669.

Secco, R. A. (1995), Viscosity of the outer core, in *Handbook of Physical Constants*, edited by T. J. Ahrens, pp. 218–226, AGU, Washington.

Senft, L. E., and S. T. Stewart (2009), Dynamic fault weakening and the formation of large impact craters, *Earth Planet. Sci. Lett.*, *287*, 471–482.

- Stevenson, D. J. (1987), Limits on lateral density and velocity variations in the Earth's outer core, *Geophys. J. R. Astron. Soc.*, *88*, 311–319.
- Stevenson, D. J., T. Spohn, and G. Schubert (1983), Magnetism and thermal evolution of the terrestrial planets, *Icarus*, *54*, 466–489.
- Watters, W. A., M. T. Zuber, and B. H. Hager (2009), Thermal perturbations caused by large impacts and consequences for mantle convection, *J. Geophys. Res.*, *114*, E02001, doi:10.1029/2007JE002964.
- Weiss, B. P., et al. (2002), Records of an ancient Martian magnetic field in ALH84001, *Earth Planet. Sci. Lett.*, *201*, 449–463.
- Weiss, B. P., L. E. Fong, H. Vali, E. A. Lima, and F. J. Baudenbacher (2008), Paleointensity of the ancient Martian magnetic field, *Geophys. Res. Lett.*, *35*, L23207, doi:10.1029/2008GL035585.
- Williams, J.-P., and F. Nimmo (2004), Thermal evolution of the Martian core: Implications for an early dynamo, *Geology*, *32*, 97–100, doi:10.1130/G19975.1.
- Yoder, C. F., A. S. Konopliv, D. N. Yuan, E. M. Standish, and W. M. Folkner (2003), Fluid core size of Mars from detection of the solar tide, *Science*, *300*, 299–303.
- Young, R. E., and G. Schubert (1974), Temperature inside Mars: Is the core liquid or solid?, *Geophys. Res. Lett.*, *1*.
- Zuber, M. (2001), The crust and mantle of Mars, *Nature*, *412*, 220–227.

---

J. Arkani-Hamed, Department of Physics, University of Toronto, Toronto, ON M5S 1A7, Canada. (jafar@physics.utoronto.ca)

P. Olson, Earth and Planetary Sciences, Johns Hopkins University, Baltimore, MD 21218, USA.